

An electrostatic actuator for fatigue testing of low-stress LPCVD silicon nitride thin films

Wen-Hsien Chuang^a, Rainer K. Fettig^b, Reza Ghodssi^{a,*}

^a MEMS Sensors and Actuators Lab (MSAL), Department of Electrical and Computer Engineering and the Institute for Systems Research, University of Maryland, College Park, MD 20742, USA

^b NASA Goddard Space Flight Center, Greenbelt, MD 20771, USA

Received 22 June 2004; accepted 8 March 2005

Available online 28 April 2005

Abstract

An electrostatic actuator and mechanical-amplifier (MA) device has been designed and fabricated to study fatigue properties of low-stress LPCVD silicon nitride thin films. The device consists of two resonators connected serially with a common torsion bar. When pumping electrostatic energy into the first resonator, the energy is transferred to the second resonator via the common torsion bar. The mechanical movement of the second resonator is thus amplified, introducing high stress levels (up to 7.7 GPa) when actuated at its first resonant mode. All devices were tested inside a focused-ion-beam (FIB) system with pressure of 10^{-6} Torr at room temperature (23 ± 1 °C), and the test duration ranged from 5 s to 8.5 h, 10^5 to 10^9 cycles, respectively. An ANSYS finite-element-analysis (FEA) model was built to determine the maximum operating stress of the devices. From the experiment, no failure of low-stress LPCVD silicon nitride thin films has been found even up to 10^9 cycles when testing at stress amplitude below 5.8 GPa with a load ratio of 0.03. The presented device design and experimental technique can be used to characterize fatigue properties of different microelectromechanical systems (MEMS) materials, and the test results are utilized in the design of microshutter arrays, programmable field selectors in the NASA James Webb Space Telescopes (JWST).

© 2005 Elsevier B.V. All rights reserved.

Keywords: Silicon nitride; Fatigue; Electrostatic actuator; MEMS

1. Introduction

Due to the rapid innovation of microelectromechanical systems (MEMS) technologies over the last few decades, a variety of innovative micro-scale machines and sensors have been developed. Associated with these advances in design, fabrication, and packaging of microsystems is an expansion of the set of materials available to MEMS designers. In order to ensure performance and reliability of MEMS devices for long periods of time, it has become increasingly important to understand the time- and cycle-

dependent degradation of MEMS materials in their operating environment.

Fatigue, the failure of a material at less than its ultimate strength after a number of cyclic loadings, is the most important and commonly encountered mode of failure in structural materials. Mechanisms for the fatigue of ductile and brittle materials at macro-scale have been generally established after a century of research. However, the study of bulk materials in fatigue failure can not be directly applied to MEMS structures [1–3].

The characterization of fatigue properties on the micro-scale is challenging due to the small dimensions of test devices. In previous research, several test devices were designed and fabricated. Bagdahn and Sharpe [4] developed a 3.5 μm thick and 50 μm wide tensile specimen under tension–tension cyclic loadings to study reliability of polycrystalline silicon.

* Corresponding author. Present address: A.V. Williams Building, Room 1357, University of Maryland, College Park, MD 20742, USA.
Tel.: +1 301 405 8158; fax: +1 301 314 9281.

E-mail address: ghodssi@eng.umd.edu (R. Ghodssi).

Similar micro-structures were adopted for cyclic loadings of LIGA (an acronym of lithography, electroplating, and molding) nickel films [5]. Although the direct tension test is an effective method for fatigue characterization, the requirements for strain measurement and sample alignment are stringent. Another approach is to integrate test specimen and setups with electrostatic actuation on the same chip. Ballarini et al. fabricated arrays of comb actuators with a notch, operating at their resonant modes during the test [6]. The deformation of the specimen, which would be converted into propagation of the crack at the notch, was recorded during the experiment. Their analysis was based on measured deformations and extensive finite-element-analysis (FEA) modeling. Van Arsdell and Brown used resonating circular comb drive actuators with a notch to detect damage under repeated loadings according to the same operation principle [7]. However, all these techniques mainly focused on conductive polycrystalline silicon thin films.

Currently, two dimensional microshutter arrays are being developed at NASA Goddard Space Flight Center (GSFC), to be used as programmable field selectors for a multi-object spectrometer (MOS) on the James Webb Space Telescope (JWST) [8,9]. The elements of the microshutter arrays were made of LPCVD silicon nitride thin films with suspended torsion bars (Fig. 1). Since the JWST operates in outer space, making maintenance extremely complicated, a complete understanding of mechanical properties and reliability issues is critical for the development of the microshutter arrays.

This paper presents a design of electrostatic test devices (mechanical-amplifier (MA) devices) with dimensions similar to the elements of the microshutter arrays to emulate torsional operating stress for fatigue study of low-stress LPCVD silicon nitride thin films. In order to obtain different stress levels without high applied voltage, mechanical amplification of mechanical-amplifier devices was achieved using a resonant technique. Additionally, all experiments were performed inside a focused-ion-beam (FIB) system based on a designed measurement setup. The presented device design, fabrication processes, and experimental techniques are suitable for characterizing fatigue properties of a number of

MEMS materials and can be extended for different MEMS applications.

2. Device design

For most MEMS devices, the maximum stress level during operation is usually kept low to prevent fracture or fatigue failure at an early stage. Instead, to study fatigue properties of structural materials, the stress level must be high enough and controllable. Among different actuation mechanisms in MEMS devices, electrostatic actuation is utilized in this study since it can provide fast response and relatively simple fabrication processes. However, the usage of electrostatic actuation to achieve high stress level is challenging due to the limitation of applied voltage across a fixed gap. If the gap between two electrodes is increased, the required amplitude of applied voltage becomes extremely high to actuate these structures. On the other hand, if the gap is small, there is not enough room for movement to introduce high stress levels to structures.

In our device design, a mechanical-amplifier device based on the concept of coupled resonators [10,11] is proposed as shown in Fig. 2. Two resonators are connected serially with a common torsion bar to address the limitation of electrostatic actuation discussed above. When operating, electrostatic energy is applied to *resonator 1* and this energy is transferred to *resonator 2* with a common torsion bar. The vibration of *resonator 2* is then amplified by its quality factor when the frequency of pumped energy matches its resonant frequency, inducing high stress levels on the torsion bar. Based on this operation principle, the vibration amplification and amplitude of *resonator 2* can be controlled by the frequency and amplitude of the input electrostatic energy, respectively. In this design, *fixed beam 1* is used to increase lateral stiffness to prevent non-torsional movement on the torsion bar without significant energy loss during operation. The dimensions of our mechanical-amplifier devices are presented in Table 1.

An analytic model is developed to estimate the stress level on a mechanical-amplifier device. For a given torque T applied to a torsion bar, the maximum shear stress can be

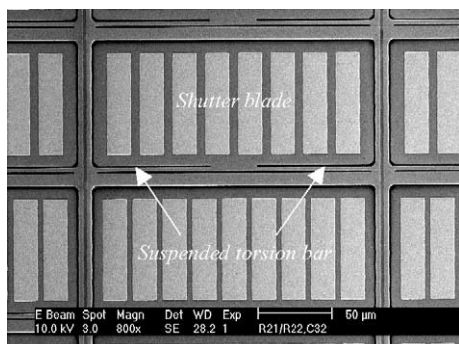


Fig. 1. Micrograph of a microshutter array fabricated at NASA GSFC.

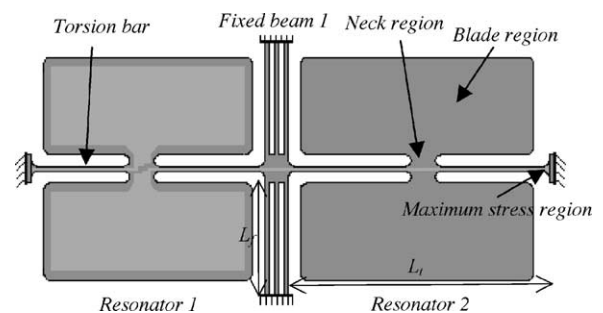


Fig. 2. Schematic diagram of a mechanical-amplifier device for fatigue testing.

Table 1
Dimensions of mechanical-amplifier devices

Torsion bar (μm)		Blade region (μm)		Neck region (μm)		Fixed-beam 1 (μm)		Thickness (μm)
L_t	W_t	L_b	W_b	L_n	W_n	L_f	W_f	T
108	2	95	35	15	5	40.5	0.8	0.5

expressed as [12]

$$\tau_{\max} = \frac{3T}{8ab^2} \left[1 + 0.6095 \frac{b}{a} + 0.8865 \left(\frac{b}{a} \right)^2 - 1.8023 \left(\frac{b}{a} \right)^3 + \left(\frac{b}{a} \right)^4 \right] \quad \text{for } a \geq b \quad (1)$$

where a is half the long edge of the rectangular section and b is half the short edge. The torque T is related to the twist angle θ by

$$T = \frac{\theta KG}{L} \quad (2)$$

and

$$K = ab^3 \left[\frac{16}{3} - 3.36 \frac{b}{a} \left(1 - \frac{b^4}{12a^4} \right) \right] \quad (3)$$

here, L is the torsion bar length and G , the modulus of rigidity. The above equations neglect the stress concentration at the end of the torsion bars, and are only applied to predict maximum shear stress of *resonator 2* as shown in Fig. 2.

3. Fabrication

The fabrication process begins with a thin silicon wafer ($250 \mu\text{m}$) coated with $0.5 \mu\text{m}$ thermal oxide and $0.5 \mu\text{m}$ low-stress LPCVD silicon nitride (residual stress of silicon ni-

tride: $183.4 \pm 14.7 \text{ MPa}$) as shown in Fig. 3. A layer of 50 \AA chromium and a layer of 500 \AA gold are deposited and patterned using a sputtering system and wet etching (chromium and gold etchants), respectively, to form the electrodes on *resonator 1*. Device structures are then defined on a silicon nitride thin film using reactive ion etching (RIE). Front-to-back alignment is performed to determine the open windows for deep reactive ion etching (DRIE) on the backside of the wafer. The front side of the wafer is then bonded to a handle wafer using photoresist to protect metal layers from further processes. Silicon nitride and thermal oxide in the open windows on the backside are removed by RIE and buffered oxide etch (BOE), respectively. The silicon substrate is etched through from the open windows using DRIE. The thin thickness of silicon wafers used in this experiment provides a more accurate etch profile control with thermal oxide as an etch stop layer during DRIE process. Finally, the thermal oxide (etch stop) is removed with BOE and the wafer is released from the handle wafer. The mechanical-amplifier device after fabrication is shown in Fig. 4.

4. Experimental techniques

4.1. FIB system with a measurement setup

In our previous work, a measurement setup was designed and installed inside a FIB system to characterize Young's

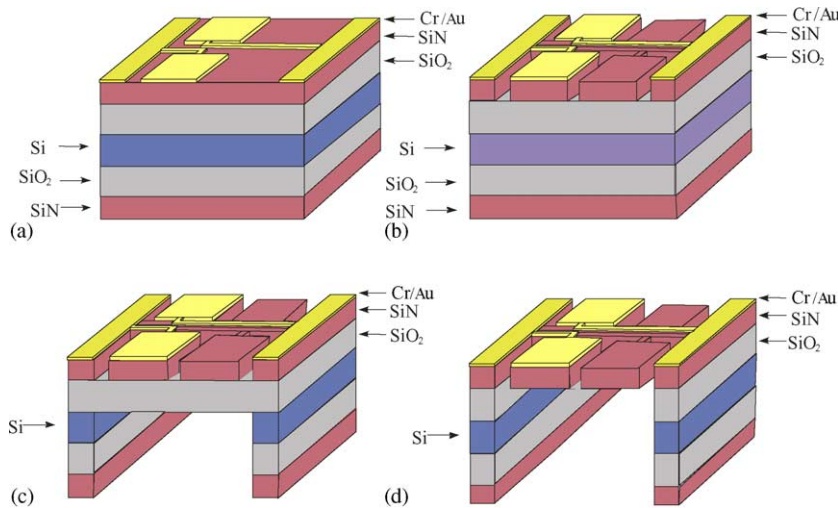


Fig. 3. Process flow of device fabrication. (a) Chromium/gold deposition and patterning for the electrodes of *resonator 1* (first mask). (b) Defines the test structure on SiN using reactive ion etching (second mask). (c) Patterns the backside and use DRIE to etch through thin silicon substrate (third mask). (d) Removes the oxide layer (etch stop of DRIE).

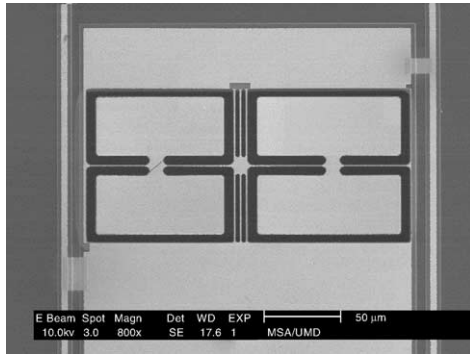


Fig. 4. Micrograph of a mechanical-amplifier device after fabrication.

modulus and fracture strength of LPCVD silicon nitride thin films at cryogenic temperatures [13]. The FEI 620 FIB used in our experiment is a dual beam system, with ion and electron columns, permitting ion milling and in situ scanning electron microscopy (SEM). This system also has the ability to deposit platinum (Pt) by ion-induced metal-organic-chemical-vapor deposition (MOCVD) [14].

Fig. 5 shows the configuration of the measurement setup inside the FIB system. A lead-zirconate-titanate (PZT) translator powered by a DC voltage was attached to a G-10 (thermal and electrical insulator) plate. The G-10 plate was then fixed on a 3-D stage controlled by three stepper motors. A small G-10 tube (10 mm in length, 3.5 mm in diameter, and 0.6 mm in wall thickness) was attached on the top surface of the PZT translator. A micro-needle, for use as a ground electrode in actuating mechanical-amplifier devices (discussed in the next section), was mounted to the metal part of the G-10 tube with a copper wire as an electrical conduction path. The combination of the PZT translator and the 3-D stage provides the capability to manipulate the micro-needle. In addition, the device stage shown in Fig. 5 can be rotated and tilted.

4.2. Vibration frequency determination

In the FIB system, an SEM image is formed by collecting the secondary electron signal when a fine electron beam is

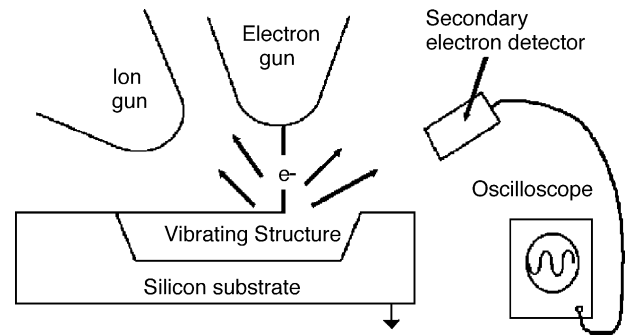
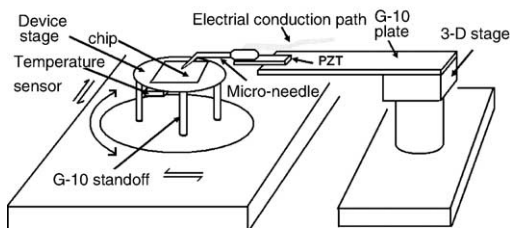


Fig. 6. Schematic diagram of the mechanism for vibration frequency determination.

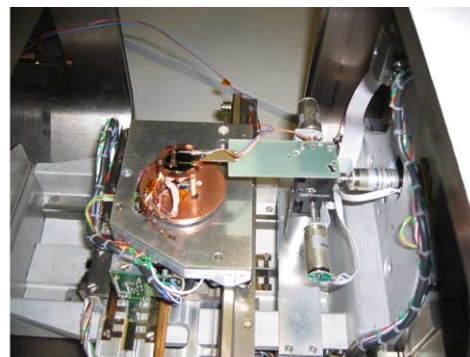
scanned over the surface of a specimen. The collected secondary electron signal varies with the topography and composition of the specimen. This principle can be applied to measure vibrating frequencies of a mechanical-amplifier device. Instead of scanning over the whole surface, a point electron beam is placed in a fixed position where the vibrating blade of a mechanical-amplifier device moves in and out of the electron beam path. This modulates the secondary electron signal with the frequency of vibration and this signal is acquired with an oscilloscope to determine the vibrating frequency. The mechanism of the vibration frequency determination inside the FIB system is shown in Fig. 6.

4.3. Micro-needle ground electrode

In the configuration of a mechanical-amplifier device, a ground electrode under or above the electrodes of *resonator 1* is required to actuate this device. One possible solution to fabricate this ground electrode is to utilize the silicon substrate under *resonator 1*. In this case, the DRIE etching step mentioned in Fig. 3 would only remove the silicon from under *resonator 2*. The thermal oxide under *resonator 1* is utilized as a sacrificial layer and could be etched away using a surface micromachining technique to release the structure of *resonator 1*. However, the disadvantages of this method are the requirement of a heavily doped silicon substrate and a more complicated fabrication process.



(a)



(b)

Fig. 5. Configuration of the measurement setup: (a) schematic view and (b) photograph of the system.

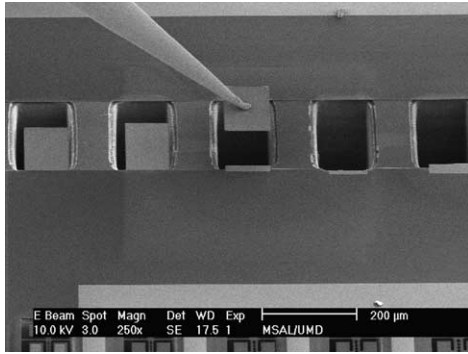


Fig. 7. Micrograph of a micro-needle welded to a nitride membrane coated with a chromium/gold layer.

An alternative approach is to use a micro-needle ground electrode as shown in Fig. 7. The micro-needle mentioned previously is positioned to contact with a silicon nitride membrane coated with a chromium/gold layer. This needle is then welded to this membrane using ion-induced platinum deposition. This micro-needle with membrane was then released by milling away the connecting parts of the membrane to the substrate to form a ground electrode. The advantages of this method are the freedom to move the ground electrode and a relatively simple fabrication process of mechanical-amplifier devices.

4.4. Testing procedure

When testing a mechanical-amplifier device, the micro-needle ground electrode was positioned above *resonator 1* with an appropriate height (approximately 5–8 μm) and connected to electrical ground. Two AC voltages (sinusoidal waveforms) with 90° phase difference were applied to the electrodes on *resonator 1*, causing the blades of *resonator 1* to alternatively move up and down. The pumped electrostatic energy was then transferred to *resonator 2* via the common torsion bar and drove it at its first resonant mode. The first resonant mode was determined by sweeping a range of frequencies around the expected value and monitoring the vibrating amplitude of *resonator 2*. Once the resonant mode was obtained, the device was excited at this frequency with fixed input voltage amplitude for a set period of time. Afterwards, the frequency response was again evaluated by sweeping around the excitation frequency. Over time, this permits measuring any change in resonant frequency due to the accumulation of fatigue damage. Given the well-established properties (Young's modulus, Poisson ratio, and density) of low-stress LPCVD silicon nitride thin films and the vibrating amplitude of *resonator 2*, the maximum stress on the structure can be determined from an ANSYS FEA model. Therefore, the relationship between fatigue life and stress is obtained.

For a given twist angle θ , the maximum shear stress can be increased by varying the dimensions of a torsion bar as shown in (1). However, the current design of the mechanical-amplifier devices was intended to emulate the operation of

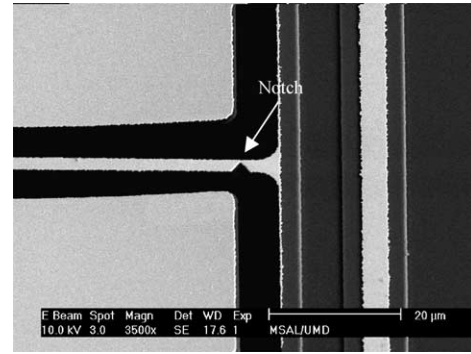


Fig. 8. Micrograph of a mechanical-amplifier device with a notch on the torsion bar.

microshutter devices with the same dimensions. Therefore, to further increase the stress level without dimensional modifications, a mechanical-amplifier device with a notched torsion bar was adopted in this study (Fig. 8). The notch structures used here were defined using ion milling with low ion energy of 5 keV and small milling current of 4 pA.

5. Results and discussion

All devices were tested in a controlled environment (pressure: 10^{-6} Torr, temperature: 23 ± 1 °C) with input voltages varied from 8.8 V_{rms} to 28.3 V_{rms} using the testing procedure described above, while the test duration ranged from 5 s to 8.5 h, or 10^5 to 10^9 cycles. Fig. 9 shows a mechanical-amplifier device with *resonator 2* at its first resonant mode. In this experiment, the input voltages to *resonator 1* were 10.6 V_{rms} and the resonant frequency of *resonator 2* was found to be 33.258 kHz. The corresponding resonant spectrum of *resonator 2* is presented in Fig. 10. In addition, mechanical amplification between *resonator 1* and *resonator 2* is shown in Fig. 11. In this figure, small movement of *resonator 1* introduces large vibration of *resonator 2* based on the principle described previously. ANSYS FEA models (Fig. 12) with dimensions of the mechanical-amplifier device were built to calculate the maximum stress on a torsion bar

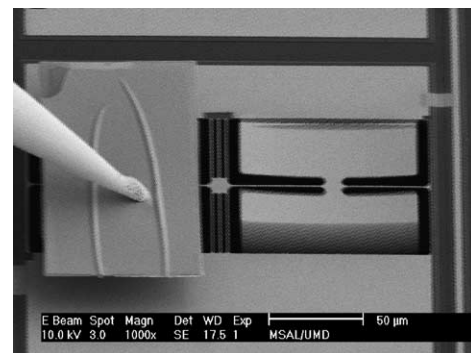


Fig. 9. Micrograph of a mechanical-amplifier device under testing with *resonator 2* at its first resonant mode.

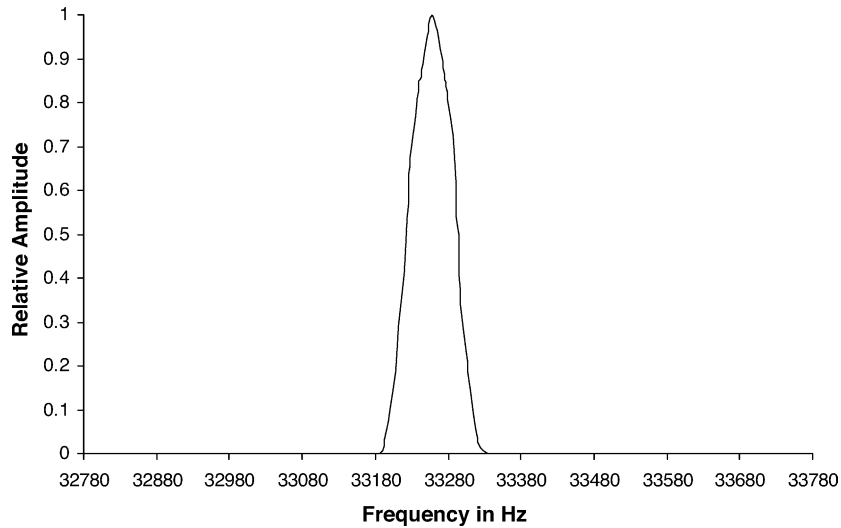


Fig. 10. Resonant spectrum of resonator 2 shown in Fig. 9.

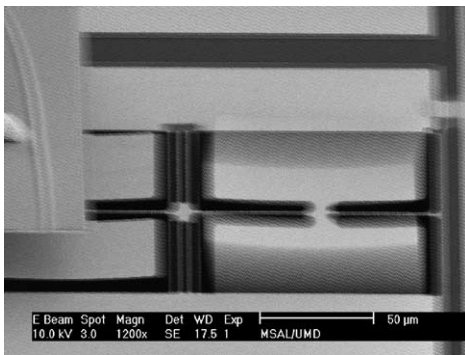


Fig. 11. Micrograph of a mechanical-amplifier device to demonstrate mechanical amplification.

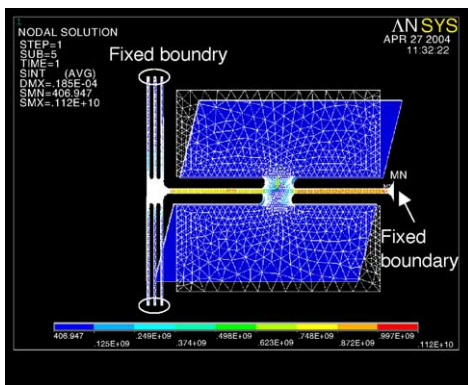


Fig. 12. ANSYS FEA model used to calculate maximum stress on a torsion bar for a given blade displacement. Circles in this figure represent a fixed boundary.

for a given blade displacement, measured directly inside the FIB. The elements and parameters utilized in these models are presented in Table 2. Here, the stress concentration at the ends of a torsion bar with a radius of curvature $r = 1.5 \mu\text{m}$ was simulated. Similarly, the notch tip radius was measured using SEM function and represented by a radius of curvature $r = 0.2 \mu\text{m}$ in the FEA model. Linear and nonlinear analyses, with different mesh sizes, were performed for each data point to verify that there is no geometric effect in these models. The simulation results showed a linear increase of stress amplitude at small displacement (within $12 \mu\text{m}$) and both linear and nonlinear analyses gave the same results. At higher blade displacement, the stress amplitude from the nonlinear analysis is larger than that from the linear analysis, which is in agreement with the nonlinear stiffening effect. Fig. 13 presents the maximum operating stress on a torsion bar for different blade displacements according to these ANSYS models. From this figure, the mechanical-amplifier device with a notched torsion bar shows higher stress amplitude as a result of the introduced notched stress concentration.

Results from the stress-life testing of low-stress LPCVD silicon nitride are shown in Fig. 14. When testing at the maximum operating stress over 6.6 GPa, the mechanical-amplifier devices exhibited time-delay failure. On the other hand, the mechanical-amplifier devices survived cyclic loadings even up to 10^9 cycles at lower operating stress. The resonant frequencies of these devices (at lower stress amplitude) were used to monitor variation of stiffness but no deviation of these frequencies was observed during experiment. Therefore, when subjected to sinusoidal, cyclic stress with amplitude below 5.8 GPa and a load ratio of 0.03, the

Table 2
Element and parameters of silicon nitride thin films utilized in ANSYS FEA model

Element	Density (kg/m^3)	Young's modulus (GPa)	Poisson's ratio	Residual stress (MPa)
Solid-92/solid-187	3000 [15]	260.5 [13]	0.23 [16]	183.4

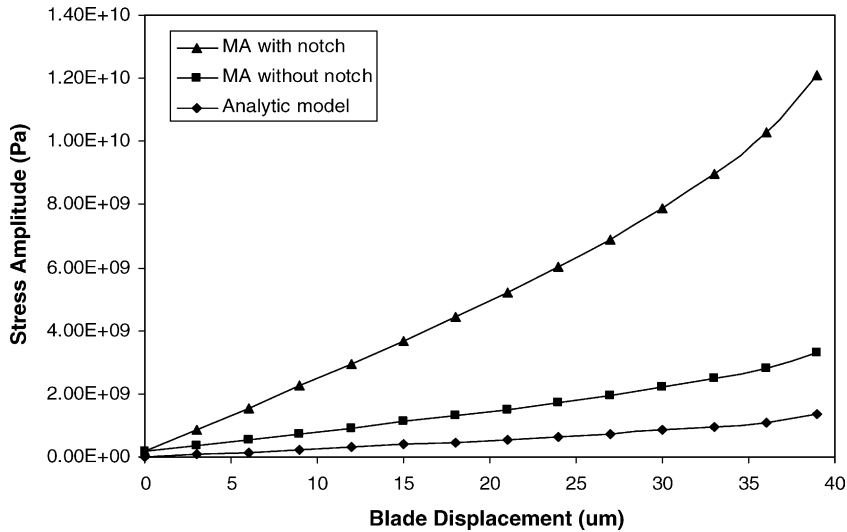


Fig. 13. Maximum operating stress with different blade displacements from ANSYS FEA model and analytic model.

low-stress LPCVD silicon nitride thin films did not display time-dependent degradation or failure up to 10^9 cycles in the testing environment. The fatigue failure of polycrystalline silicon in ambient air has been observed in previous study [17]. The fatigue process is attributed to a mechanism involving the environmentally-assisted cracking of the surface oxide film, and similar phenomena may exist for premature failure of silicon nitride materials. However, our experiments were performed in a vacuum environment, so this mechanism is not applicable to our work. As the surface condition of test structures is a critical factor to induce premature failure, the observed damage on the notched torsion bar after ion milling can increase local stress amplitude and initiate a crack, which may explain the short lifetime of the test devices.

The microstructure of a fatigue specimen (Fig. 15) using low voltage SEM was used to establish the mode of crack advance without altering the surface by coating with conductive layers. The crack was observed to initiate at the notch tip (identified by a different morphology of the fracture surface) and propagate along the remaining ligament of the notched torsion bar. Layer structures parallel to the direction of crack propagation and unidentified debris were found on the fracture surface, which are the proof of cyclic damage. An additional thin silicon dioxide layer was observed at the bottom of the cross-section due to incomplete etching of the etch stop after DRIE process.

During the experiment, the maximum blade displacement of *resonator 2* was found to be 32 μm . The limitation was

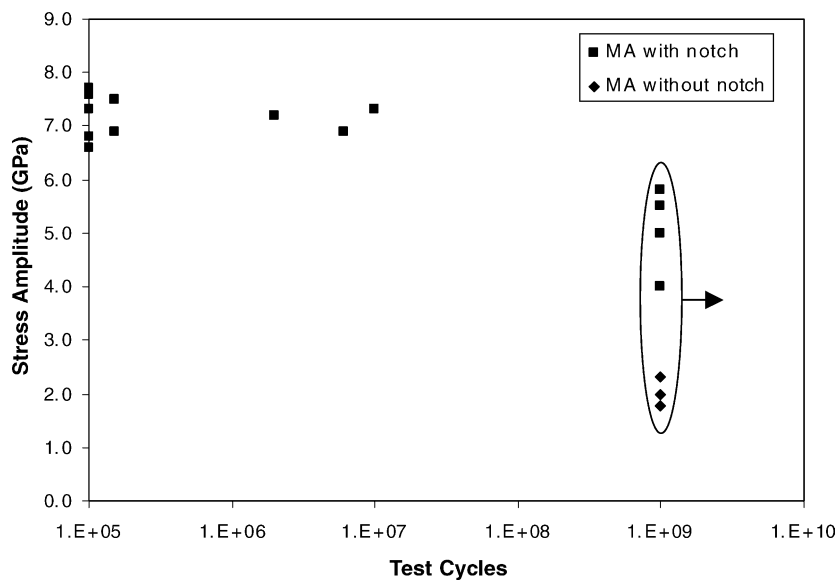


Fig. 14. Stress-life testing data for low-stress LPCVD silicon nitride. When testing at high stress level, test devices exhibited time-delayed failure. Conversely, the circle with a horizontal arrow indicates devices that did not fail under cyclic loadings up to 10^9 cycles when testing at lower stress amplitude.

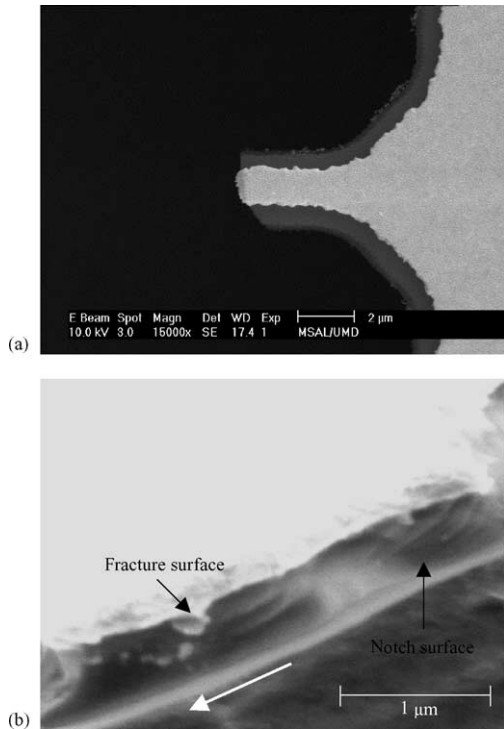


Fig. 15. (a) Micrograph of a notched torsion bar that failed after ~ 6 million cyclic loadings at stress amplitude of 6.8 GPa. (b) Micrograph of the fracture surface after cyclic loadings. The arrow (white color) indicates the direction of crack propagation.

caused by pull-in energy loss and intrinsic material damping. For high input voltages, the blades of *resonator 1* tried to pull in with the micro-needle ground electrode. Instead of making torsional motion on a torsion bar, most energy was used to create up-and-down movement which was compensated by *fixed-beam 1* and became ineffective in actuating *resonator 2*. Several uncertainties may cause errors in the determination of maximum operating stress from the ANSYS FEA models. First, the cross sections of torsion bars are not perfectly rectangular due to the fabrication process. The curvature of these bars is difficult to measure, especially for thin film materials. Second, the small variation of curvature at the notch tip and the influence of chromium/gold thin films were not considered in these models. Third, *resonator 1* was neglected in the FEA model for simplicity due to its relatively small movement. In addition, the applied voltages to the test devices disturbed electron beam signals and caused distortion of scanning electron micrographs. This may introduce errors in the measurements of blade displacements. However, based on the current design of the mechanical-amplifier device, *resonator 2* vibrates only when the frequency of the applied voltages is close to its resonant mode. This mechanism can be utilized as a calibration method by measuring the blade displacement of a static *resonator 2* with the same applied voltages (but not at the resonant frequency). Furthermore, the test devices were tilted with an angle (52°) for better observation of vibration ampli-

tude during experiments. The corresponding error in stress measurement due to the distorted images is estimated to be less than 0.4 GPa.

The fracture strength of silicon nitride thin films from our previous study is 6.9 GPa [13]. However, no fracture failure was observed even when the device was tested at stress amplitude higher than the reported fracture strength. This can be explained by the increase of the fracture strength of the silicon nitride composite structure (silicon nitride coated with chromium and gold layers) [18]. The usage of low ion energy and chromium or gold protective layers during ion milling process has been demonstrated to minimize FIB-induced damage [19,20]. Even so, it is inevitable to introduce gallium implantation and surface damage on the notched torsion bars, which may decrease fatigue resistance at high operating stress in our study. However, the test results can provide conservative stress amplitude for reliability design of a microstructure using silicon nitride thin films in a vacuum environment.

The operation of the microshutter arrays requires 90° rotation of shutter blades to achieve open states, which induce a maximum operating stress of 3.5 GPa on the torsion bars. In addition, the number of cycles expected in the lifetime of microshutter arrays is 10^5 [21]. From this study, even though the FIB-induced damage may reduce fatigue lifetime, the mechanical-amplifier devices with notch structures still survived 10^9 cyclic loadings at a maximum operating stress of 5.8 GPa. Therefore, the microshutter devices are not expected to display fatigue failure during their operation. Although the microshutter devices will operate at cryogenic temperatures (30–35 K) in outer space, the thermally induced mismatch stress between the low-stress LPCVD silicon nitride membrane and the metal coating layer is not likely to result in failure due to the thin coating thickness. Thermal stress and fatigue properties of the composite structures used in the microshutter devices at cryogenic temperatures are under investigation to confirm the reliability of the microshutter arrays at these reduced temperatures.

6. Conclusions

This paper presents the design, fabrication, and fatigue testing of an electrostatic actuator. Mechanical amplification was demonstrated using a resonant technique. All devices were tested inside a FIB system (pressure: 10^{-6} Torr, temperature: $23 \pm 1^\circ\text{C}$) based on a designed measurement setup and developed experimental techniques. Additionally, ANSYS FEA models were used to calculate the maximum operating stress of these devices during testing. From the stress-life experiment, no fatigue failure of low-stress LPCVD silicon nitride thin films was found even up to 10^9 cycles when testing at stress amplitude below 5.8 GPa with a load ratio of 0.03. Further characterization of silicon nitride thin films at cryogenic temperatures is currently underway.

Acknowledgements

This work was funded by NASA Goddard Space Flight Center (GSFC) under grant NAG512011. The authors would like to thank the microshutter group at NASA GSFC for providing microshutter devices, Nolan Ballew for the help in using cleanroom facility, and John Barry for the assistance in using the FIB system at University of Maryland. The authors would also like to acknowledge Thomas Luger and John Pyle for their contributions to the measurement setup.

References

- [1] C.L. Muhlstein, S.B. Brown, R.O. Ritchie, High-cycle fatigue of single-crystal silicon thin films, *J. Microelectromech. Syst.* 10 (2001) 593–600.
- [2] C.L. Muhlstein, E.A. Stach, R.O. Ritchie, Mechanism of fatigue in micro-scale films of polycrystalline silicon for microelectromechanical systems, *Appl. Phys. Lett.* 80 (2002) 1532–1534.
- [3] R.O. Ritchie, Mechanisms of fatigue-crack propagation in ductile and brittle solids, *Int. J. Fract.* 100 (1999) 55–83.
- [4] J. Bagdahn, W.N. Sharpe, Fatigue of polycrystalline silicon under long-term cyclic loading, *Sens. Actuators A* 103 (2003) 9–15.
- [5] H.S. Cho, K.J. Hemker, K. Lian, J. Goettert, Tensile, creep and fatigue properties of LIGA nickel structures, in: *Proceedings of the Fifteenth IEEE International Conference on Micro Electro Mechanical Systems*, 2002, pp. 439–442.
- [6] R. Ballarini, R.L. Mullern, H. Kahn, A.H. Heuer, *The Fracture Toughness of Polysilicon Microdevices*, vol. 518, Materials Research Society, San Francisco, CA, 1998, pp. 137–142.
- [7] W. Van Arsdell, S.B. Brown, Crack growth in polysilicon, in: *Proceedings of the ASME International Mechanical Engineering Congress and Exposition*, vol. 66, Anaheim, CA, 1998, pp. 267–272.
- [8] S.H. Moseley, R.K. Fettig, A. Kutylev, C. Bowers, R. Kimble, J. Orloff, B. Woodgate, Programmable 2-dimensional microshutter arrays, in: *Proceedings of SPIE* 3878, 1999, pp. 392–397.
- [9] S.H. Moseley, R.K. Fettig, A. Kutylev, M. Li, D. Mott, B. Woodgate, Status of the development of a 128 X 128 microshutter array, in: *Proceedings of SPIE* 4178, 2000, pp. 51–58.
- [10] L. Lin, R.T. Howe, A.P. Pisano, Microelectromechanical filters for signal processing, *J. Microelectromech. Syst.* 7 (1998) 286–294.
- [11] F.D. Bannon, J.R. Clark, C.T.-C. Nguyen, High-Q HF microelectromechanical filters, *J. Microelectromech. Syst.* 35 (2000) 512–526.
- [12] W.C. Young, *Roark's Formulas for Stress and Strain*, McGraw-Hill, 1989.
- [13] W.-H. Chuang, T. Luger, R.K. Fettig, R. Ghodssi, Mechanical property characterization of LPCVD silicon nitride thin films at cryogenic temperatures, *J. Microelectromech. Syst.* 13 (2004) 870–890.
- [14] J. Orloff, M. Utlaut, L. Swanson, *High Resolution Focused Ion Beams*, Kluwer, 2002.
- [15] S.D. Senturia, *Microsystem Design*, Kluwer, 2001.
- [16] H.D. Pierson, *Handbook of Chemical Vapor Deposition: Principles, Technologies, and Applications*, William Andrew, 1999.
- [17] C.L. Muhlstein, S.B. Brown, R.O. Ritchie, High-cycle fatigue and durability of polycrystalline silicon thin films in ambient air, *Sens. Actuators A* 94 (2001) 177–188.
- [18] J.-A. Schweitz, Mechanical characterization of thin films by micro-mechanical techniques, *MRS Bull.* (1992) 34–45.
- [19] B.W. Kempshall, L.A. Giannuzzi, B.I. Prenitzer, F.A. Stevie, S.X. Da, Comparative evaluation of protective coatings and focused ion beam chemical vapor deposition processes, *J. Vac. Sci. Technol. B* 20 (2002) 286–290.
- [20] S. Rubanov, P.R. Munroe, FIB-induced damage in silicon, *J. Microsc.* 214 (2003) 213–221.
- [21] A.S. Kutylev, S.H. Moseley, R.A. Boucarut, M. Jhabvala, M. Li, D.S. Schwiger, R.F. Silverberg, R.P. Wesenberg, Programmable microshutter arrays for the jwst nirspec, in: *Proceedings of the 2003 IEEE/LEOS International Conference on Optical MEMS*, 2003, pp. 87–88.

Biographies

Wen-Hsien Chuang received the BS and MS degrees in electrical engineering from the National Cheng Kung University, Tainan, Taiwan, in 1995 and 1997, respectively. Since August 2001, he joined the MEMS Sensors and Actuators Lab (MSAL) at the University of Maryland and began working toward the PhD degree. His current research, in collaboration with NASA Goddard Space Flight Center (GSFC), focuses on design, fabrication, and cryogenic characterization of MEMS materials and devices for space applications. Mr. Chuang is a student member of the IEEE, AVS and MRS societies.

Rainer K. Fettig is an independent scientist working on various aspects of microstructures for space flight applications. He received a Diploma in Physics and the degree Dr. rer. nat. from the University of Karlsruhe, Germany in 1986 and 1993, respectively. Between 1989 and 1996 he headed a team that developed built and delivered thermoelectric infrared detectors for the focal plane 1 of the CIRS instrument on board CASSINI, a NASA mission to Saturn. Between 1996 and 2002 he worked at NASA Goddard Space Flight Center on several projects to develop microstructures for optical applications. He played a major role in the development of microshutters, one of NASA's most visible MEMS projects. In 2002, he returned to Karlsruhe for private reasons and spent a year at the Research Center Karlsruhe to develop nanohole optical filters produced in a modified LIGA process. Dr. Fettig is freelancing since July 2003.

Reza Ghodssi received his BS, MS, and PhD degrees in electrical engineering from the University of Wisconsin at Madison, in 1990, 1992 and 1996, respectively. Dr. Ghodssi was a Postdoctoral Associate and a Research Scientist in the Microsystems Technology Laboratories and the Gas Turbine Laboratory at the Massachusetts Institute of Technology (MIT) from 1997 until 1999. During his tenure at MIT, he developed the building block MEMS fabrication technologies for a microturbine generator device and also served as an Assistant Director on that project. Dr. Ghodssi is Director of the MEMS Sensors and Actuators Laboratory (MSAL) and an Associate Professor in the Department of Electrical and Computer Engineering and the Institute for Systems Research (ISR) at the University of Maryland (UMD). He is also a core faculty member in the Bioengineering Graduate Program and Small Smart Systems Center (SSSC) at UMD. His research interests are in design and development of microfabrication technologies and their applications to microsensors, microactuators and integrative microsystems. He was awarded the 2001 UMD George Corcoran Award, 2002 National Science Foundation CAREER Award and the 2003 UMD Outstanding Systems Engineering Faculty Award. Dr. Ghodssi has served as a program co-chairman for the 2001 International Semiconductor Device Research Symposium (ISDRS) and as a chairman of the MEMS and NEMS Technical Group at the American Vacuum Society (AVS), from 2002 to 2004. Dr. Ghodssi is a co-founder of the MEMS Alliance Group in the greater Washington area and a member of the IEEE, AVS, MRS, AAAS and ASEE societies.